Shear horizontal acoustic waves propagating along two isotropic solid plates bonded with a non-dissipative adhesive layer: Effects of the rough interfaces

Catherine Potel, Michel Bruneau, Ludovic Cardin Foze Ndjomo, Damien Leduc, Mounsif Echcherif Elkettani, Jean-Louis Izbicki

AIP Journal of Applied Physics

Shear horizontal acoustic waves propagating along two isotropic solid plates bonded with a non-dissipative adhesive layer: Effects of the rough interfaces

Catherine Potel, Michel Bruneau, Ludovic C. Foze N'Djomo, Damien Leduc, Mounsif Echcherif Elkettani, and Jean-Louis Izbicki

Citation: Journal of Applied Physics **118**, 224904 (2015); doi: 10.1063/1.4937150
View online: http://dx.doi.org/10.1063/1.4937150
View Table of Contents: http://scitation.aip.org/content/aip/journal/jap/118/22?ver=pdfcov
Published by the AIP Publishing

Shear horizontal acoustic waves propagating along two isotropic solid plates bonded with a non-dissipative adhesive layer: Effects of the rough interfaces

Catherine Potel,[1,2,a)] Michel Bruneau,[1,2] Ludovic C. Foze N'Djomo,[1,2] Damien Leduc,[2,3] Mounsif Echcherif Elkettani,[2,3] and Jean-Louis Izbicki[2,3]
[1]*Laboratoire d'Acoustique de l'Université du Maine (LAUM, UMR CNRS 6613), 72000 Le Mans, France*
[2]*Fédération d'Acoustique du Nord Ouest (FANO, FR CNRS 3110), France*
[3]*Laboratoire Ondes et Milieux Complexes (LOMC, UMR CNRS 6294), 76058 Le Havre, France*

(Received 16 April 2015; accepted 22 November 2015; published online 11 December 2015)

The aim of this paper is to provide an analytical contribution which presents the application of shear-horizontal (SH)-guided waves for the characterisation of a bi-layered structure which consists of two isotropic plates adhesively bonded using a non-dissipative thin layer of glue. The thickness of the layer of glue is assumed to be non-negligible, and the interfaces between this layer of glue and the plates are both assumed to be roughened (parallel ridges with complex shape and depth profiles). The basis of the theoretical approach is an extension of the integral formulation, in the frame of SH modal couplings due to the roughness, which has been developed previously for SH-wave propagation over a single plate with a rough surface. This approach assumes that the average roughness height is a small fraction of the thicknesses of the waveguides (the plates) everywhere. The changes, due to the roughness, in the characteristics of the fields created by a harmonic source set at the entrance edge of the structure are expressed through the mapping of the displacement and stress perturbations. Preliminary tests of the effectiveness of the model are given; they rely on the phase-matching effects of periodic profiles and pseudo-random experimental profile. © *2015 AIP Publishing LLC*. [http://dx.doi.org/10.1063/1.4937150]

I. INTRODUCTION

The nature and properties of ultrasonic waves within elastic waveguides are topics of enduring importance in fundamental acoustics and its practical applications. The literature abounds with many papers in which topics of principal focus involve guided waves techniques to non-destructively characterize the engineering components. Such techniques become particularly relevant whenever adhesive bonded components (increasingly used in engineering applications) are concerned.[1–3]

Many researches have been produced on the general topic of ultrasonic non-destructive evaluation (NDE) of adhesive bonds, using mainly either Lamb or Shear-Horizontal (SH) guided waves.[4,5] Most of the literature deals with the characterization of the adhesive properties at the bonded interfaces. We can quote, among others, characterization and evaluation of adhesion, detection of defects, and lack of adhesion.[6–12] Concerning the rheological models used to describe the behavior of the glue and the interfaces between it and the structure, mainly two basic models are involved: a cohesive rheological model that corresponds to the standard approach in which the entire adhesive layer is replaced by a spring surface, and an adhesive rheological model which consists in describing only the contact zones by a spring surface distribution (among inertia and dissipation).[13,14] Indeed, the cohesive rheological model makes it possible to quantify global (cohesive) defects in the adhesive layer, while the adhesive rheological model targets local (adhesive) defects on the interface level.

Concerning the literature on the related subjects, one can mention also articles that address the effects of complex structures with rapid change of curvatures at the interfaces and boundaries, including those which involve periodically undulated interfaces between waveguides. Several theoretical methods are used: they include semi-analytical methods (like the distributed point source method), method of multiple scales, or Green's tensor for fields in half space.[15–21] It is worth noting also that the class of problem mentioned above is common in others fields (optic, electromagnetism, underwater acoustics, atmospheric propagation, duct acoustics, etc.)[22–28] and bibliography therein. Besides, guided SH-waves have been successfully used to characterise the roughness of the surface of isotropic plates in using the same basic formalism as the one used herein,[29] which could be particularly relevant before applying adhesive joints. Therefore, it is of interest to understand the behaviour of SH-waves propagating along a multi-layered structure consisting of two isotropic plates glued together when complex shapes and depth profiles of the roughness affect the characteristics of the structure, thereby motivating the use of a new modelling.

As mentioned above, in much of the more practical recent literature, the theoretical work is extensively numerical,[13,14,30] relying on finite element programs based on available packages. Such approach is capable of modelling complex problem, but it could inhibit insight which can be offset if one has some benchmark analytical solution.

[a)]Author to whom correspondence should be addressed. Electronic mail: Catherine.Potel@univ-lemans.fr. Tel.: 33 2 43 83 36 17. Fax: 33 2 43 83 35 20.

Actually, these analytical solutions are for specialized geometries, and their implementation could involve extensive numerical calculation, but they could remain advantageous in the analysis of the behaviour observed. On the other hand, several authors investigate physical properties of bonded structures in using also analyses which rely on the dispersion or phase velocity curves.[7,16,31–33] Here, the paper provides an analytical model which enables to express the perturbation of the displacement field and the stress fields in the structure considered, considering both the depth and the shape of the roughness.

The main goal of this paper is to provide such an analytical model for SH-waves propagating along two plates stuck together, each having the same lateral dimensions but different thicknesses and material properties, the surfaces pasted being roughened. More precisely, this analytical contribution presents the application of SH-guided waves for the characterisation of a multi-layered structure which consists of two isotropic plates adhesively bonded using a non-dissipative thin layer of glue described by a shear-spring model, the interfaces between this layer of glue and the plates being both assumed to be roughened (parallel ridges with complex shape and depth profiles). The part of the plates stuck together behaves not really as a bilaminar plate comprised of two perfectly bonded elastic plates, because the thickness of the layer of glue is assumed to be non-negligible.

The basis of the theoretical approach is the integral formulation which has been developed previously[34,35] for SH-wave propagation along a plate with a rough surface. This approach assumes that the average roughness height is a small fraction of the thicknesses of the waveguides (the plates) everywhere. The development that follows involves the modification of waveguide SH-modes which occurs when roughness is involved. The behaviour of the acoustic field perturbed by the roughness is presented mainly in terms of both SH modal couplings inside each plate and SH modal couplings between the plates through the layer of glue. The changes, due to the roughness, in the characteristics of the fields created by a harmonic source set at the entrance edge of the structure are expressed through the mapping of the displacement and stress perturbations. Preliminary tests of the effectiveness of the model are given; they rely on the phase-matching effects of periodic profiles and pseudo-random experimental profile.

The formulation gives a prominent role to an integral formulation (involving a suitable Green's function), in which the field perturbation is expressed as an expansion on an orthogonal set of functions involving a finite number of non-perturbed SH-modes. Therefore, after the presentation of the three layered structure (Section II), the paper is divided in three parts: the analytical modelling of the SH modes without roughness (Section III), the integral formulation for the field scattered by the roughness along with the resultant approximate solutions (Section IV), while supplementary details are relegated to Appendix C, and finally (Section V), the results, mainly the mapping of the displacement fields and the stress fields and their perturbation due to the roughness.

II. THE MULTILAYERED STRUCTURE (THREE LAYERS)

The structure considered in the following (see Fig. 1) is a two dimensional set of two homogeneous parallel plates (labelled $q = 1, 2$) adhesively bonded using a thin layer of glue, the interfaces between this layer of glue and the plates being both roughened (ridges parallel to the y-axis herein). The structure is assumed to be infinite in the y-direction, set in vacuum, and bounded by two parallel plane surfaces perpendicular to the z-direction. A SH-wave, polarized along the ridges (parallel to the y-axis), is assumed to propagate along the x-axis parallel to the external surfaces of the structure.

Introducing a coordinate system in each plate $q = 1, 2$, labelled (x_q, z_q), each vertical axis z_q having its origin O_q in the middle of the plate and being directed towards the rough surface of the considered plate (Fig. 1), the coordinates of the ridged surfaces (which depend on the coordinate x defined above) are given, respectively, by $z_q = Z_q(x)$. Each plate is assumed to be bounded by two parallel surfaces perpendicular to the z-axis, set, respectively, at the coordinates $z_q = \pm L_q/2$ $(L_q > 0)$. Therefore, denoting $h_q(x) > 0$ the depth of the corrugations, the coordinates of the corrugated surfaces can be written as follows: $Z_q(x) = (L_q/2) - h_q(x)$. The shapes of these ridged surfaces are defined by their unit vectors $\mathbf{n}_q$ normal to the surfaces of the plates, directed outward from the plate interior, given by

$$\mathbf{n}_q = N_q^{-1}[(\mathrm{d}_{x_q} h_q)\mathbf{e}_{x_q} + \mathbf{e}_{z_q}] = N_q^{-1}[(\mathrm{d}_x h_q)\mathbf{e}_x + (-1)^{q+1}\mathbf{e}_z], \tag{1a}$$

with $N_q = \sqrt{1 + (\partial_x h_q)^2}$, $\mathbf{e}_{x_q} = (-1)^{q+1}\mathbf{e}_x$ and $\mathbf{e}_{z_q} = (-1)^{q+1}\mathbf{e}_z$ denoting the unit vectors that have, respectively, the positive direction of the x_q- and z_q-coordinates.

Inner plates of thicknesses $d_q > 0$ with regularly shaped surfaces are defined in such a way that the corrugations are trapped between the surfaces $z_q = L_q/2$ and $z_q \cong d_q/2$ $(h_q \ll d_q)$. Denoting $L_g > 0$ the thickness of the layer of glue between the fictive planes $z_q = L_q/2$, it follows that the sum

$$\begin{aligned} \ell_g(x) &= L_g + h_1(x) + h_2(x) \\ &= L_g + [(L_2/2) - Z_2(x)] + [(L_1/2) - Z_1(x)], \end{aligned} \tag{1b}$$

represents the thickness of the layer of glue (which depends on the coordinate x). Note that each layer is characterized by its density and its shear second Lamé coefficient,

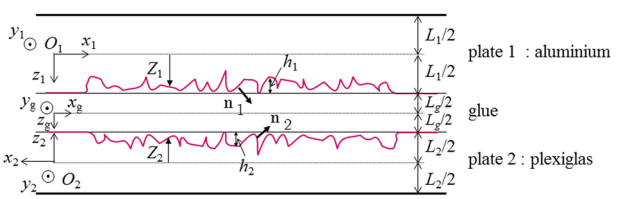

FIG. 1. Sketch of the 2D structure with smooth upper and lower surfaces, and with rough interfaces between each plate and the thin layer of glue.

respectively, ρ_q and μ_q for the plates, and ρ_g and μ_g for the layer of glue.

III. THE ANALYTICAL MODELLING

A. The basic equations

A harmonic [with a time factor $\exp(\mathrm{i}\,\omega\,t)$], incident propagating SH-wave coming from the left end of the structure (Fig. 1), is characterised by its amplitude (depending on the coordinate z) at the entrance $x = 0$ of the ridged plate [domains D_q, $x \in (0, \infty)$, $z_q \in (-L_q/2, Z_q)$]. The shear displacement fields in each plate $(q = 1, 2)$, assumed to be polarized along the y-axis (along the ridges), are denoted

$$\hat{\mathbf{u}}_q(x, z_q; t) = \hat{U}_q(x, z_q)\, \exp(\mathrm{i}\omega t)\, \mathbf{e}_y, \tag{2}$$

where $\mathbf{e}_y$ ($\mathbf{e}_y = \mathbf{e}_{y_1} = \mathbf{e}_{y_2}$) denotes the unit vector that has the positive direction of the y-coordinate, and $\hat{U}_q(x, z_q)$ represents the y-component of the complex amplitude of the displacement field. Their behaviours are governed by the set of equations, including the propagation equation and the boundary conditions, which takes the following form:

$$\begin{cases} (\partial^2_{xx} + \partial^2_{z_q z_q} + k_q^2)\ \hat{U}_q(x, z_q) = -\hat{f}(z_q)\,\delta(x), & [x,\ z_q] \in D_q, & \text{(3a)} \\ \overline{\overline{\mathbf{T}}}_q(x, z_q)\,.\,\mathbf{n}_q = 0, \quad \forall x \in (0, \infty), & z_q = -L_q/2, & \text{(3b)} \\ \left.\begin{array}{l} \overline{\overline{\mathbf{T}}}_q(x, z_q)\,.\,\mathbf{n}_q = \overline{\overline{\mathbf{T}}}_g(x, z_q)\,.\,\mathbf{n}_q \\ \hat{U}_q(x, z_q) = \hat{U}_g(x, z_q) \end{array}\right\}, & x \in (0, \infty), \quad z_q = Z_q(x), & \begin{array}{l}\text{(3c)}\\ \text{(3d)}\end{array} \\ \text{No wave coming back from } +\infty, & & \text{(3e)} \end{cases}$$

where $k_q = \omega/c_q$, $c_q = \sqrt{\mu_q/\rho_q}$ being the speed of the shear waves in the homogeneous solid plates, $\hat{f}(z_q)$ represents the source strength at $x = 0$ [$\delta(x)$ being the Dirac function], and $\overline{\overline{\mathbf{T}}}_q(x, z)$ and $\overline{\overline{\mathbf{T}}}_g(x, z)$ represent the stress tensors, respectively, in the plates and the glue.

Invoking the Hooke's law and accounting for the polarization along the y-axis of the SH-wave, the boundary conditions (3b) and (3c) on the ridged surfaces involve the following expression:

$$\overline{\overline{\mathbf{T}}}_q(x, z_q)\,.\,\mathbf{n}_q = \mu_q \partial_{n_q} \hat{U}_q(x, z_q)\, \mathbf{e}_y, \tag{4}$$

with

$$\overline{\overline{\mathbf{T}}}_q(x, z_q)\,.\,\mathbf{n}_q = N_q^{-1}[T_{yx}(x, z_q)\,(\mathrm{d}_x h_q) + (-1)^{q+1}\, T_{yz}(x, z_q)]\ \mathbf{e}_y, \tag{5}$$

and where

$$\partial_{n_q} = \mathbf{n}_q.\nabla = N_q^{-1}[(\mathrm{d}_{x_q} h_q)\,\partial_{x_q} + \partial_{z_q}] = N_q^{-1}[(\mathrm{d}_x h_q)\,\partial_x + (-1)^{q+1}\partial_z], \tag{6}$$

is the normal derivative with respect to the normal $\mathbf{n}_q$ directed outward from the plate interior. Note that when the slope of the roughness tends to infinity, this expression (6) remains finite. Equivalent expressions for the parameters involving the index "g" follow from the same definitions and the same properties.

To express the behaviour of the glue, we assume that the thickness $\ell_g(x)$ of the layer of glue is very thin (but it does not vanish): it remains much smaller than the inverse of the z-component of the wavenumber k_{z_q}. Then, neglecting the effects of inertia of this thin layer of glue, i.e., assuming the zero order approximation with respect to the thickness $\ell_g(x)$ of the following basic equation, namely (see the orientation of the z_q-axis):

$$0 \cong \ell_g\, \rho_g \partial^2_{tt} U_1 \cong \ell_g\, \rho_g \partial^2_{tt} U_2 \cong \mu_1 \partial_{n_1} U_1(x, z_1 = Z_1) + \mu_2 \partial_{n_2} U_2(x, z_2 = Z_2), \tag{7a}$$

which implies that the stress tensor is uniform over this layer, and neglecting other effects (dissipation, relaxation, etc.), the behaviour of this layer of glue can be expressed by a classical spring-like model (Jones' model), with a spring stiffness (μ_g/ℓ_g)

$$\mu_q \partial_{n_q} \hat{U}_q = -\mu_{s\neq q} \partial_{n_{s\neq q}} \hat{U}_{s\neq q} = \frac{\mu_g}{\ell_g}\left[\hat{U}_{s\neq q}(x', Z_s) - \hat{U}_q(x', Z_q)\right]. \tag{7b}$$

This interface condition between the plates,[36,37] described by a shear-spring model (the stress is continuous but the displacement is not), is successfully employed when the layer of the glue is very thin (which is usually the case in practice).

B. Zero order approximation: Two plates with smooth surfaces and with a thin layer of glue

In this subsection, we assume that $Z_q(x) = (L_q/2)$ $(q = 1, 2)$ and $\ell_g(x) = L_g$, i.e., $h_q(x) = 0$ (no roughness). In each plate, the displacement fields $\hat{U}_q(x, z_q)$ propagating along the x-axis, denoted in this subsection (no roughness) $\hat{U}_q^{(0)}(x, z_q)$, takes the following form, accounting for the boundary condition $\overline{\overline{\mathbf{T}}}_q(x, z_q)\,.\,\mathbf{n}_q = 0$ at the outer surfaces of the plates $z_q = -L_q/2$ (here, $\mathbf{n}_q = -\mathbf{e}_{z_q}$):

$$\hat{U}_q^{(0)}(x, z_q) = 2\, C_q^{(0)} \exp(\mathrm{i}k_{z_q}^{(0)} L_q/2)\, \cos k_{z_q}^{(0)}(z_q + L_q/2)\, \exp(-\mathrm{i}k_x^{(0)} x), \tag{8a}$$

with

$$k_{z_q}^{(0)} = \sqrt{k_q^2 - (k_x^{(0)})^2} \neq 0, \tag{8b}$$

$C_q^{(0)}$ denoting the amplitudes of the fields which depend on the strength of the source.

Then, the continuity conditions at the interfaces $z_q = -L_q/2$, $q = 1, 2$ (Equation (7b)) give two homogeneous algebraic equations for the unknown amplitudes $C_1^{(0)}$ and $C_2^{(0)}$. The determinant of the square matrix associated to this couple of equations must vanish (details are given in Appendix A). This leads to the following equation (dispersion equation) which allows expressing the longitudinal x-components $k_{x_M}^{(0)}$ of the wavenumber (the z-component of the wavenumber $k_{z_q}^{(0)} \equiv k_{z_q M}^{(0)}$ and the integration constants have also to be thought of as labelled "$M = 1, 2, 3, ...$" below):

$$\frac{L_1/\mu_1}{\left(k_{z_1 M}^{(0)} L_1\right)\tan\left(k_{z_1 M}^{(0)} L_1\right)} + \frac{L_2/\mu_2}{\left(k_{z_2 M}^{(0)} L_2\right)\tan\left(k_{z_2 M}^{(0)} L_2\right)} - \frac{L_g}{\mu_g} = 0. \tag{9}$$

IV. INTEGRAL FORMULATION

A. Orthonormal modes and Green's function for each plate

The solution of Equations (3) will be expressed (through an integral formulation, see Section IV B) in the frame of an expansion of a finite number of SH-modes, using a set of relevant one-dimensional orthogonal, normalised, functions $\psi_{q_m}(z_q)$ $(m = 0, 1, 2, ..., M_{\max})$ at a given frequency, for each two-dimensional waveguide bounded by the regularly shaped, parallel, and plane surfaces set at $z_q = \pm L_q/2$. The incident displacement field $U_{q_I}^{(0)}(x, z)$, assumed in Section V to be a given SH-mode "I" at a given frequency, undergoes scattering on the roughened surfaces, initiating all the SH-modes $U_{q_M}^{(0)}(x, z)$ which can take place in the process (in the frame of Born approximation). This set of SH-modes, given in Section III, does not satisfy standard orthogonality conditions. Then, in order to express the perturbed field as an expansion involving this finite number of SH-modes, an orthonormal set of functions is retrieved from them on using the Gram-Schmidt process.[38] This method for orthonormalising the set of SH-modes, which span any displacement fields possible as a superposition of the existing SH modes at the given frequency, is presented in Appendix B.

Note that the orthogonal normalised functions $\psi_{q_m}(z_q)$ do not depend on the x-coordinate and that the index $m = 0$ is chosen to label the incident SH-mode $M = I$, the other modes being then ordered sequentially.

The solution method of Equation (3) (integral formulation presented below) involves an appropriate Green's function, at a given frequency, in each plate in the absence of roughness, corresponding to a point source located at a position (x', z'_q) in the plate labelled "q," which does not depend on the SH-mode considered. The Green's function chosen is required to satisfy the following relations, in the domain $D_{q_0} = [x \in (0, \infty), z_q \in (-L_q/2, L_q/2)]$:

$$\begin{cases} [\partial^2_{x_q x_q} + \partial^2_{z_q z_q} + k_q^2]\, G_q(x_q, z_q; x'_q, z'_q) = -\delta(x_q, x'_q)\ \delta(z_q, z'_q),\ z_q \in (-L_q/2,\ L_q/2), & \text{(10a)} \\ \partial_{z_q} G_q(x_q, z_q; x'_q, z'_q) = 0, \quad z_q = -L_q/2, & \text{(10b)} \end{cases}$$

The Green's function which obeys this system of equations (10) has the explicit form[39,40]

$$G_q\left(x_q, z_q; x'_q, z'_q\right) = -\frac{\mathrm{i}}{4}\{H_0^-(k_q|\,\mathbf{r}_q - \mathbf{r}'_q\,|) + H_0^-(k_q|\,\mathbf{r}_q - \mathbf{r}''_q\,|)\}, \tag{11a}$$

with

$$|\,\mathbf{r}_q - \mathbf{r}'_q\,| = \sqrt{(x_q - x'_q)^2 + (z_q - z'_q)^2},$$
$$|\,\mathbf{r}_q - \mathbf{r}''_q\,| = \sqrt{(x_q - x'_q)^2 + (z_q - z''_q)^2},$$
$$z''_q = (z'_q + L_q), \tag{11b}$$

where H_n^- denotes the first Hankel function of order "n."

It is noteworthy that this cylindrical Green's function $G_q(\mathbf{r}_q, \mathbf{r}'_q)$ and its derivative have a singularity at $\mathbf{r}_q = \mathbf{r}'_q$. But it is readily verifiable that, despite this integrand singularity which occurs in the integrals below (Section IV B), the limits of the integrations are finite.

It should be emphasized that the Green's function does not satisfy any interface condition on the plane surface $z_q = L_q/2$ and that the interface condition for the SH fields is applied on the rough boundary $z_q(x) = Z_q(x)$, denoted below $z_q(x') = Z'_q$.

B. The integral formulation

With both the Green function (11) and the displacement field $\hat{U}_q(x, z_q)$ satisfying the same Neumann boundary condition at the outer surface $(-L_q/2)$ of each plate, the integral formulation equivalent to the problem inside the plates stated above (3a)–(3d), which involves domains

$$D_{q_0} = [x \in (0, \infty), z_q \in (-L_q/2, L_q/2)] \quad \text{and}$$
$$D_q = [x \in (0, \infty),\ z_q \in (-L_q/2, Z_q)],$$

can be written as follows (the source term being described by an adapted function $\hat{S}_q(z_q)$ at the entrance $x_0 = 0$ of each plate):[39,40]

$$\left.\begin{array}{ll}(x,\, z_q) \in (D_q), & \hat{U}_q(x,\, z_q) \\ (x,\, z_q) \in (D_{q_0} - D_q), & 0 \end{array}\right\} = \int_{-L_q/2}^{L_q/2} G_q(x_q, z_q; x_0, z'_q)\hat{S}_q(z'_q)\mathrm{d}z'_q + \int_0^{+\infty} [\, G_q(x,\, z_q; x',\, Z'_q)\, \partial_{n'_q} \hat{U}_q(x',\, Z'_q) - \hat{U}_q(x',\, Z'_q)\, \partial_{n'_q} G_q(x,\, z_q; x',\, Z'_q)\,]\, \mathrm{d}\, x'\,. \quad (12)$$

This approach can be considered as an extension of the one used previously to describe successfully the effect of the roughness on the propagation of SH-waves in a single plate. But the derivations presented below depart deeply from the previous one because, while appropriate to addressing the example of single plate, they fail when the coupling between glued plates is considered.

Note that, owing to the choice of the Green's functions (boundary conditions on the outer surfaces set at $z = -L_q/2$), the integral over these surfaces vanish. Then, the remaining integral over the surfaces $z = +L_q/2$ in Eq. (12) permits to express analytically the scattering on the roughness.

It is noteworthy that the perturbed displacement field due to the scattering on the roughness represents both the self-coupling of the incoming mode with itself and the cross-coupling between this incident SH-wave and the other modes which can exist at the working frequency.

On assuming that the energy transfer from the external source to the plate "q," represented by the first integral in the right hand side of Equation (12), is not perturbed significantly by the scattering on the roughness (this is coherent with the usual experimental output data which are normalized to the incoming ones), Equation (12) becomes, for non-roughened plates

$$\hat{U}_q^{(0)}(x, z_q) = \int_{-L_q/2}^{L_q/2} G_q(x,\, z_q; x_0,\, z'_q)\; \hat{S}_q(z'_q)\mathrm{d}z'_q + \int_0^{+\infty} [\, G_q(x,\, z_q; x',\, L_q/2) \times \partial_{z'_q} \hat{U}_q^{(0)}(x',\, Z'_q = L_q/2) - \hat{U}_q^{(0)}(x',\, L_q/2) \times \partial_{z'_q} G_q(x,\, z_q; x',\, Z'_q = L_q/2)\,]\, \mathrm{d}\, x', \quad (13)$$

and then Equation (12) can be written as follows:

$$\left.\begin{array}{ll}(x,\, z_q) \in (D_q), & \hat{U}_q(x,\, z_q) \\ (x,\, z_q) \in (D_{q_0} - D_q), & 0 \end{array}\right\} = \hat{U}_q^{(0)}(x,\, z_q) + \int_0^{+\infty} [\, G_q(x,\, z_q; x',\, Z'_q)\, \partial_{n'_q} \hat{U}_q(x',\, Z'_q) - \hat{U}_q(x',\, Z'_q)\, \partial_{n'_q} G_q(x,\, z_q; x',\, Z'_q)\,]\, \mathrm{d}\, x' - \int_0^{+\infty} [\, G_q(x,\, z_q; x',\, L_q/2)\, \partial_{z'_q} \hat{U}_q^{(0)}(x',\, Z'_q = L_q/2) - \hat{U}_q^{(0)}(x',\, L_q/2)\, \partial_{z'_q} G_q(x,\, z_q; x',\, Z'_q = L_q/2)\,]\, \mathrm{d}\, x', \quad (14)$$

namely,

$$\left.\begin{array}{ll}(x,\, z_q) \in (D_q), & \hat{U}_{q_{(I)}}(x,\, z_q) \\ (x,\, z_q) \in (D_{q_0} - D_q), & 0 \end{array}\right\} = \hat{U}_{q_I}^{(0)}(x,\, z_q) + \int_0^{\infty} \{\delta_1[G_q(x,\, z_q; x',\, Z'_q)\, \partial_{n'_q} \hat{U}_{q_I}(x',\, Z'_q)] - \delta_2[\hat{U}_{q_I}(x',\, Z'_q)\, \partial_{n'_q} G_q(x,\, z_q; x',\, Z'_q)]\}\, \mathrm{d}\, x', \quad (15a)$$

where

$$\delta_1[G_q(x,\, z_q; x',\, Z'_q)\, \partial_{n'_q} \hat{U}_{q_I}(x',\, Z'_q)] = G_q(x,\, z_q; x',\, Z'_q)\, \partial_{n'_q} \hat{U}_{q_I}(x',\, Z'_q) - G_q(x,\, z_q; x',\, L_q/2)\, \partial_{z'_q} \hat{U}_{q_I}^{(0)}(x',\, L_q/2), \quad (15b)$$

and

$$\delta_2[\hat{U}_{q_I}(x',\, Z'_q)\, \partial_{n'_q} G_q(x,\, z_q; x',\, Z'_q)] = \hat{U}_{q_I}(x',\, Z'_q)\, \partial_{n'_q} G_q(x,\, z_q; x',\, Z'_q) - \hat{U}_{q_I}^{(0)}(x',\, L_q/2)\, \partial_{z'_q} G_q(x,\, z_q; x',\, L_q/2), \quad (15c)$$

represent the difference between the function inside the square brackets with roughness expressed on the roughened surface $z'_q = Z'_q$ and the same function [with the superscript (0)] without roughness expressed on the smooth surface $z'_q = L_q/2$.

Given the orthonormal functions $\psi_{q_m}(z_q)$ mentioned in Section IV A and displayed in Appendix A, the displacement field $\hat{U}_{q(I)}(x, z_q)$ in the domains $(D_q \subset D_{q_0})$ is expressed as an expansion on these orthonormal functions $\psi_{q_m}(z_q)$ labelled below $\psi_{q_{m_{(I)}}}(z_q)$ when the incident field is the mode denoted $M = I$, namely,

$$\hat{U}_{q(I)}(x, z_q) = \sum_{m=0}^{m_{\max}} \hat{A}_{q_{m_{(I)}}}(x)\, \psi_{q_{m_{(I)}}}(z_q), \quad (16)$$

where the coefficients $\hat{A}_{q_{m_{(I)}}}(x)$ are the unknowns of the problem and $m_{\max} = M_{\max}$.

Therefore, we assume Born approximation in the terms of order of magnitude of the thickness $h_q = L_q/2 - Z_q$ of the roughness and its slope (the higher order terms being neglected), i.e., assuming that the differences denoted $\delta_i[\bullet]\ (i = 1, 2)$ [Equations (15b) and (15c)] are much lower than the functions in the square bracket (they vanish when the thickness of the roughness tends to zero). Then, taking into account the orthogonality properties of the functions $\psi_{q_{m_{(I)}}}(z_q)$, in each plate labelled "q," the displacement field perturbation due to the scattering of the incident SH-wave labelled "I" on the roughened surfaces is given by (see Appendix C)

$$\hat{U}_{q_{(I)}}(x, z_q) - \hat{U}_{q_I}^{(0)}(x, z_q) = \sum_{m=0}^{M_{\max}} [\hat{\hat{H}}_{q_{m_{(I)}}}(x) + \hat{\hat{E}}_{q_{m_{(I)}}}(x)] \times \psi_{q_{m_{(I)}}}(z_q), \quad (17a)$$

where

$$\hat{\tilde{H}}_{q_{m_{(I)}}}(x) \cong -\int_0^{\ell} \{\delta_2[\hat{U}^{(0)}_{q_I}(x', Z'_q) \times \langle \partial_{n'_q} G_q(x, z_q; x', Z'_q) \,\|\, \psi_{q_m}(z_q)\rangle]\} \mathrm{d}x', \quad (17b)$$

$$\hat{\tilde{E}}_{q_{m_{(I)}}}(x) \cong -\frac{\mu_g}{\mu_q}\int_0^{\ell} \left\{\delta_3\left[\ell_g^{-1}\left(\hat{U}^{(0)}_{q_I}\left(x', Z'_q\right) - \hat{U}^{(0)}_{s\neq q_I}(x', Z'_s)\right) \times \left\langle G_q\left(x, z_q; x', Z'_q\right) \,\|\, \psi_{q_m}(z_q)\right\rangle\right]\right\} \mathrm{d}x', \quad (17c)$$

with

$$\langle f_1 \,\|\, f_2\rangle \cong \int_{-L_q/2}^{L_q/2} f_1(z_q) f_2(z_q)\, \mathrm{d}\, z_q, \quad (17d)$$

δ_3 being given in Eq. (C4b).

The second term in the left hand side of Equation (17a) represents the effect of the incident field, the first one in the right hand side represents the boundary modal coupling due to both the slope and the depth of the roughness, and the second one in the right hand side represents the perturbation on the coupling between the plates through the layer of glue (both due also to the shape profile and the depth of the roughness), which account for the effect of the thickness of the layer of glue (depending on the x-coordinate). It is worth noting that when the thickness of the glue vanishes, the difference between the displacements on the boundaries of the glue vanishes so that the expression

$$\ell_g^{-1}[\hat{U}^{(0)}_{q_I}(x', Z'_q) - \hat{U}^{(0)}_{s\neq q_I}(x', Z'_s)] = (\mu_q/\mu_g)\partial_{n'_q}\hat{U}^{(0)}_{q_I}(x', Z'_q), \quad (17e)$$

in the integrand of expression (17c) remains finite.

V. RESULTS AND DISCUSSION

A. Two plates with smooth surface (no roughness) and with a layer of glue (zero order approximation)

The results given in this sub-section correspond to two plates (aluminium and plexiglas) *in vacuo* stick together, the thickness of the layer of glue L_g being assumed much smaller than the thicknesses L_q of the plates. The physical parameters considered (shear second Lamé coefficient μ_q, shear wave velocity c_{Tq}, and density ρ_q) for aluminium ($q = 1$) and plexiglas ($q = 2$), and the thicknesses of the plates are given in Table I.

The dispersion curves for each plate q separately (Equation (9) with $L_{s\neq q} = L_g = 0$, namely, $\sin(k^{(0)}_{z_{qM}} L_q) = 0$) are shown in Figure 2, and the dispersion curves for the plates stuck together (Equation (9) with $L_g \neq 0$) are shown in Figure 3, the thickness of reference being chosen arbitrarily equals to the thickness L_1 of the aluminium plate (the vertical lines mark the values of the parameter $f.L_1$, and the dots mark the coordinates chosen in the results presented in Section V B).

TABLE I. Physical and geometrical parameters for aluminium plate "$q = 1$," plexiglas plate "$q = 2$," and glue "$q = g$."

	$q = 1$	$q = 2$	$q = g$
μ_q (GPa)	23.003	2.4110	1
ρ_q(kg m^3)	2705.8	1180.0	1300.0
c_{T_q}(m s^{-1})	3100.0	1429.4	877.0
L_q (mm)	2	0.5	0.08

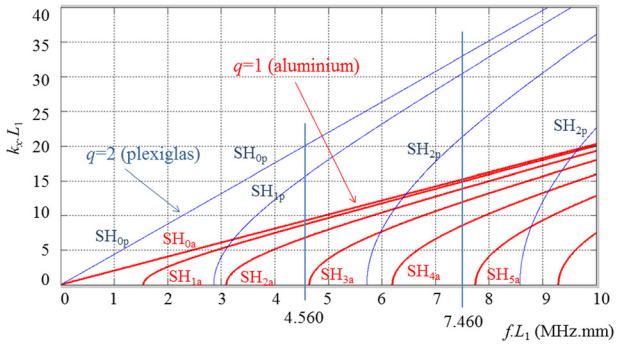

FIG. 2. Dispersion curves for each plate separately, plexiglas plate blue full thin line numbered SH_{np} and aluminium plate pink full thick line numbered SH_{na} (see Table I).

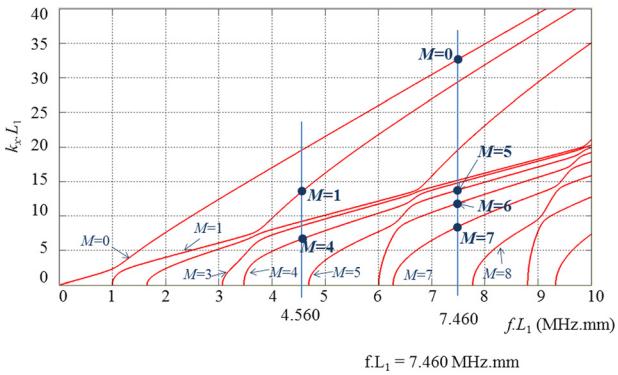

FIG. 3. Dispersion curves for the tri-layered structure (two plates and layer of glue, see Table I). The dots mark the coordinates chosen in the results presented in this paper.

Note that the values of the components $k^{(0)}_{x_M}$ and $k^{(0)}_{z_q}$ for aluminium plate "$q = 1$" and plexiglas plate "$q = 2$," when $fL_1 = 7.460$ MHz mm (corresponding to the vertical line in Figure 3), are given in Table II.

It is worth noting that all the fields presented in the remaining of the paper represent the non-dimensional ratio

$$\hat{U}^{(0)}_{q_{I=6}}/C^{(0)}_2 \quad (18)$$

TABLE II. Components $k^{(0)}_{x_M}$ and $k^{(0)}_{z_q}$ for aluminium plate "$q = 1$" and plexiglas plate "$q = 2$," when $fL_1 = 7.460$ MHz mm (see Figure 3).

Mode M	$k^{(0)}_{x_M}$ (mm^{-1})	$k^{(0)}_{z_1}$(mm^{-1})	$k^{(0)}_{z_2}$(mm^{-1})
0	16.235	−i 14.368	2.287
1	15.599	−i 12.489	7.462
2	5.642	−i 5.985	13.261
3	7.546	0.469	14.556
4	7.358	1.738	14.652
5	6.836	3.228	14.903
6	5.868	4.7666	15.310
7	4.148	6.320	15.862

for the displacement fields and the normalized stress fields defined as

$$\frac{\mu_q}{\mu_1}\,\partial_{n_q}\left[\hat{U}^{(0)}_{q\,l=6}(x,z_q)/C_2^{(0)}\right]\text{in mm}^{-1}. \tag{19}$$

Figures 4(a) and 4(b) present the mapping of the real parts of, respectively, the displacement and stress fields of SH-waves (Equation (8a)) as a function of the coordinates x and z, for a driving frequency such as the coupling between the mode SH2 in the plexiglas plate and the mode SH3 in the aluminium lead to the mode SH6 ($M = 6$) in the tri-layered structure (coordinates $fL_1 = 7.460\,\text{MHz mm}$ and $k^{(0)}_{x_M}L_1 = 11.737$, dot marked "$M = 6$" on Figure 3). The linear displacement field and the uniform stress field inside the glue are not presented on the mapping. As expected, the SH-waves are stationary in the z-direction in both plates, the displacement field shows a gap from one boundary of the glue to the other one, while the continuity of the stress field through the layer of glue appears, and the stresses vanish at the outer boundaries of the structure [it is obvious on the cuts shown in Figures 4(c) and 4(d)].

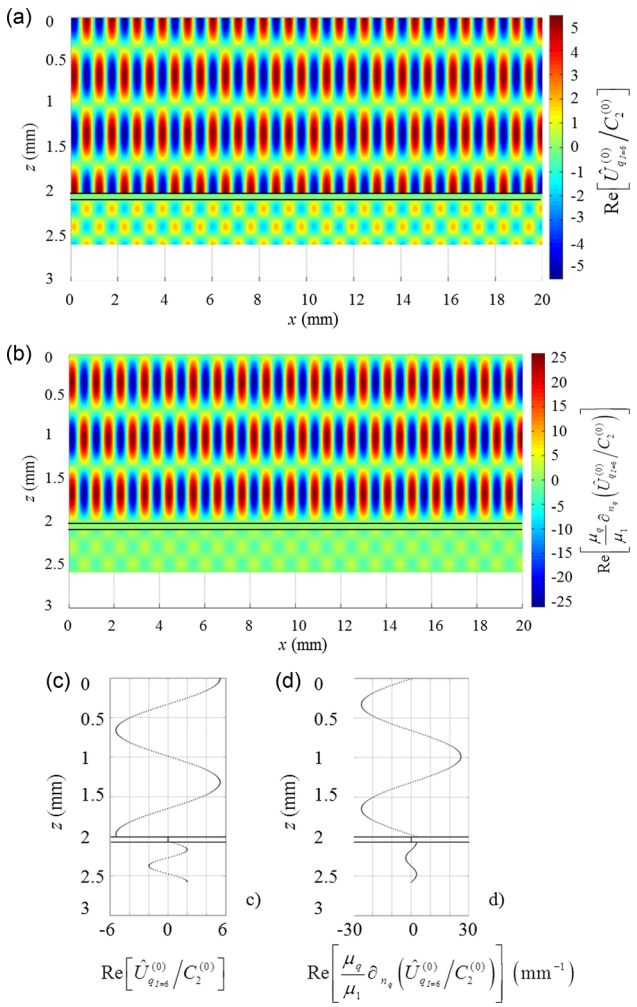

FIG. 4. Mode SH $M = 6$. Mapping of the real part of (a) the non-dimensional displacement field [Eq. (18)] and (b) the normalized stress field [Eq. (19)] for $fL_1 = 7.460\,\text{MHz mm}$ and $k^{(0)}_{x_M}L_1 = 11.737$ (dot marked $M = 6$ on Figure 3). Cuts of the maps (a) and (b), amplitudes of both the real part of the displacement field (c) and the stress field (d).

Figures 5(a) and 5(b) present the mapping of the real parts of, respectively, the displacement and stress fields of SH-waves (Equation (8a)) as a function of the coordinates x and z, for the mode SH $M = 7$ (coordinates $fL_1 = 7.460\,\text{MHz mm}$ and $k^{(0)}_{x_M}L_1 = 8.297$, lower dot marked "$M = 7$" on Figure 3). The perturbation of this mode, due to the roughness, is considered in Section V B.

For the coordinates $fL_1 = 7.460\,\text{MHz mm}$ and $k^{(0)}_{x_M}L_1 = 32.471$ (upper dot marked "$M = 0$" on Figure 3), the mapping of the real parts of, respectively, the displacement and stress fields of SH-waves (Equation (8a)) as a function of the coordinates x and z is presented, respectively, in Figures 6(a) and 6(b). As expected, the SH-waves in the plexiglas plate is stationary in the z-direction, while it is evanescent (green on the map) in the same direction in the aluminium plate.

Figures 7(a) and 7(b) present the mapping of the real parts of, respectively, the displacement and stress fields of SH-waves (Equation (8a)) as a function of the coordinates x and z, for the mode SH $M = 5$ (coordinates $fL_1 = 7.460\,\text{MHz mm}$ and $k^{(0)}_{x_M}L_1 = 13.672$, dot marked "$M = 5$" on Figure 3). The perturbation of this mode, due to the roughness, is considered in Section V B.

The results presented above can be considered as representative samples of the other situations of interest (the other results calculated, not presented herein, show the same behaviour).

B. Effect of the roughness on the behaviour of SH-waves

Being concerned by the use of the analytical approach mentioned above, results involving several roughness profiles, yet typical of applications, are presented below. Mapping of scattered waves (displacement and stress perturbations) as functions of the coordinates x and z is shown and

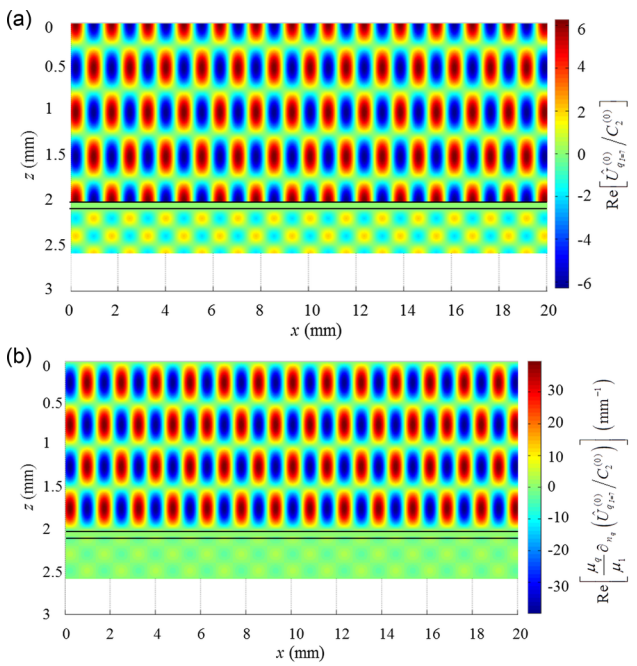

FIG. 5. Mapping of the real part of (a) the non-dimensional displacement field [Eq. (18)] and (b) the normalized stress field [Eq. (19)] of SH-waves $M = 7$ for $fL_1 = 7.460\,\text{MHz mm}$ and $k^{(0)}_{x_M}L_1 = 8.297$ (lower dot on Figure 3).

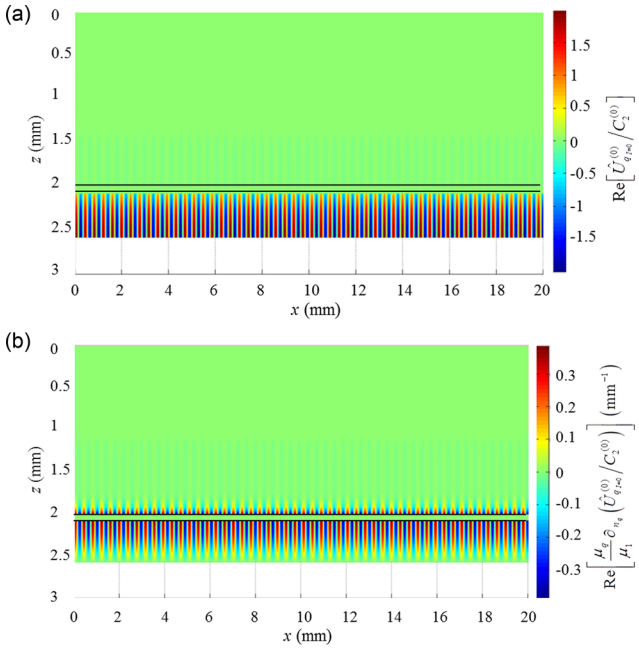

FIG. 6. Mapping of the real part of (a) the non-dimensional displacement field [Eq. (18)] and (b) the normalized stress field [Eq. (19)] of SH-waves $M = 0$ (evanescent in the aluminium plate) for $fL_1 = 7.460\,\text{MHz mm}$ and $k_{x_M}^{(0)} L_1 = 32.471$ (upper dot on Figure 3).

discussed, conveying interpretations of the physical phenomena; these maps represent either the non-dimensional ratio

$$[\hat{U}_{q_{(I)}}(x, z_q) - \hat{U}_{q_I}^{(0)}(x, z_q)]/C_2^{(0)}, \tag{20}$$

for the displacement perturbation fields or the normalized perturbation stress fields defined as

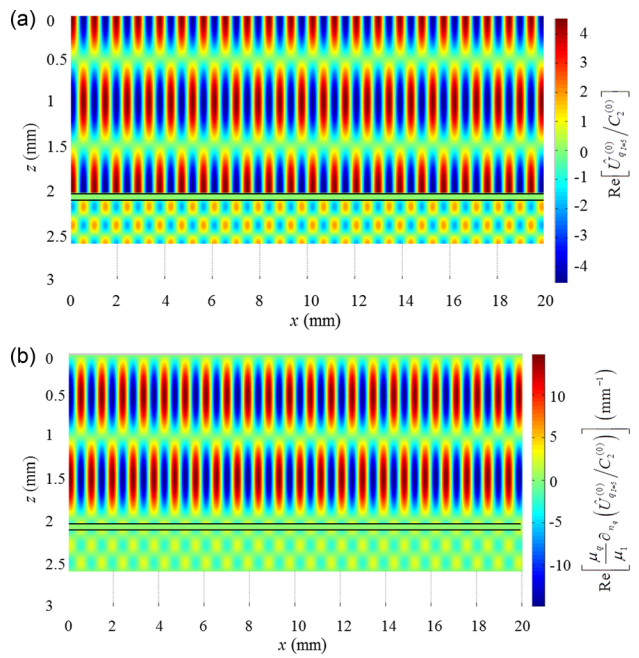

FIG. 7. Mapping of the real part of (a) the non-dimensional displacement field [Eq. (18)] and (b) the normalized stress field [Eq. (19)] of SH-waves $M = 5$ for $fL_1 = 7.460\,\text{MHz mm}$ and $k_{x_M}^{(0)} L_1 = 13.672$ (upper dot on Figure 9).

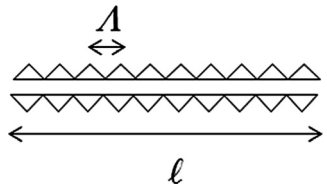

FIG. 8. Periodically sawtooth profile of finite extent $\ell = 10\,\Lambda$, depth $h/L_1 = 0.025$, and spatial period $\Lambda/L_1 = 0.314$.

$$\frac{\mu_q}{\mu_1}\,\partial_{n_q}\left(\left[\hat{U}_{q_{(I)}}(x, z_q) - \hat{U}_{q_I}^{(0)}(x, z_q)\right]\Big/ C_2^{(0)}\right) \text{in mm}^{-1}. \tag{21}$$

Two-dimensional spatial Fourier transforms of the maps in the (x, z) plane (in mm^2), leading to (k_x, k_z) diagrams, give the SH-modes which mainly contribute to the diffused field perturbations. They indicate the manner whereby the diffracted field behaves and they provide suitable basis for interpreting the maps. The conclusions which are subsequently drawn result from both the mappings in the (x, z) plane (presented in Sections V B 1 and V B 2) and the 2-D Fourier Transforms. It appears that in the examples considered in Section V B 1, different situations occur when the roughness profile is periodic, depending on whether one or two SH modes contribute preferentially to the diffused field in each plate: in the first case, it is not necessarily the same mode in both plates, and in the second case, the incident mode interferes with the mode related to it through a phonon relationship. When the roughness profile is a pseudo-random one, the perturbed field can involve more than two SH modes. For brevity, and because it suffices to illustrate the results obtained from the (k_x, k_z) diagrams, only two examples are given in terms of Fourier transform in Sections V B 1 and V B 2. The results obtained are also illustrated through the mapping of the fields and other examples are presented.

1. Mapping of scattered waves perturbations, periodic profile, phase-matching effects

The roughness considered in this subsection is a periodically sawtooth profile (isosceles triangles shown in Figure 8) of spatial period $\Lambda/L_1 = 0.314$, finite extent $\ell = 10\,\Lambda$, and depth $h/L_1 = 0.05$ (namely, here $\Lambda = 0.627\,\text{mm}$, $\ell = 6.273\,\text{mm}$, and $h = 0.05\,\text{mm}$), set symmetrically at the interfaces between the plates and the layer of glue at the entrance of the glued plates.

The so called "phonon curves," namely, here parameters $(2\,\pi L_1/\Lambda - k_{x_M}^{(0)} L_1)$ expressed as function of the variable (fL_1), are depicted in Figure 9 with $\Lambda/L_1 = 0.314$. The intersections of the dispersion curves (SH-waves numbered "I," incident) with the phonon ones (here, SH-waves numbered "M") provide the phonon relationships

$$k_{x_I}^{(0)} + k_{x_M}^{(0)} = 2\,\pi/\Lambda, \tag{22}$$

which represent the phase-matching between these SH waves. The dots mark the phase-matching between $I = 6$ and $M = 7$, $I = 7$ and $M = 6$, for a driving frequency $fL_1 = 7.460\,\text{MHz mm}$, with $k_{x_M}^{(0)} L_1 = 11.737$ and $k_{x_M} L_1 = 8.297$, respectively, and between $I = 4$ and $M = 1$ for a

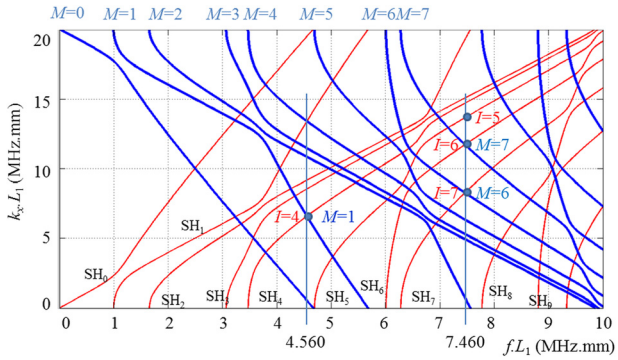

FIG. 9. Dispersion curves (red thin solid lines) and "phonon curves" (blue thick solid lines) with $\Lambda/L_1 = 0.314$; dots mark the phase matching between SH-waves.

driving frequency $fL_1 = 4.560\,\text{MHz mm}$, with $k_{x_M}L_1 = 6.639$ (see random profile in Section V B 2).

The perturbations (due to scattering on the rough surfaces) of the SH-waves considered ($I = 0$, $I = 5$, $I = 6$, and $I = 7$) are shown in Figures 10–18. These figures present the mapping of the real parts of the displacement fields perturbations (Equation (17)) and the corresponding stress fields perturbations of SH-waves as functions of the coordinates x and z.

Figures 10(a) and 10(b) present, respectively, the mapping of the real part of the displacement field perturbations (a) and the associated stress fields perturbations (b) of the incident SH6-wave ($I = 6$) created by scattering on the corrugated surfaces, for $fL_1 = 7.460\,\text{MHz mm}$ and $k_{x_6}^{(0)}L_1 = 11.737$ (dot $I = 6$ on Figure 9). For a better visibility in Figure 10(b), the color contrast in the plexiglas plate (plate 2) was enhanced by multiplying the amplitude by five (see the left scale for the aluminium plate and the right scale for the plexiglas plate). A phase-matching occurs between the incident mode SH6 and the mode SH7, for the period of the roughness considered [see

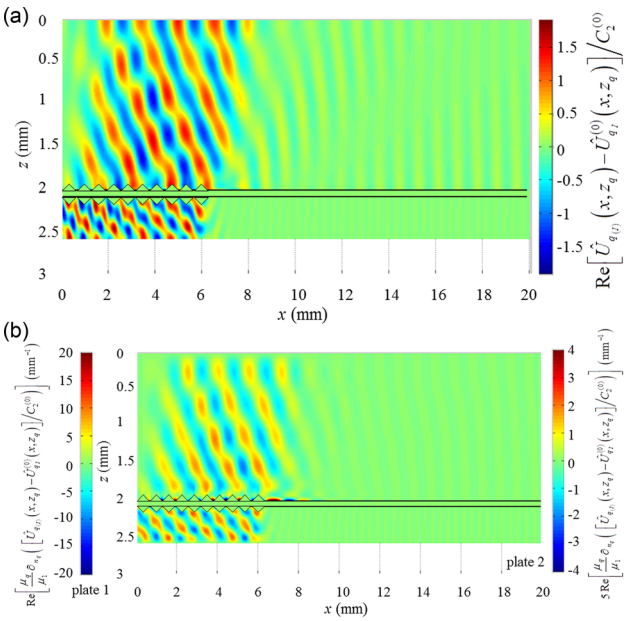

FIG. 10. Mapping of the real parts of (a) the non-dimensional displacement field [Eq. (20)] and (b) the normalized stress field [Eq. (21)] of the incident SH-wave $I = 6$ for $fL_1 = 7.460\,\text{MHz mm}$ and $k_{x_M}^{(0)}L_1 = 11.737$ (dot $I = 6$ and $M = 7$ on Figure 9).

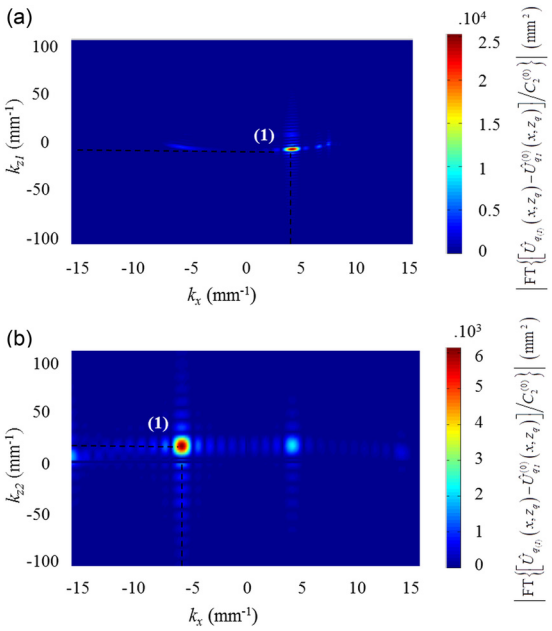

FIG. 11. Modulus of the two dimensional Fourier Transform of the map presented in Figure 10(a). (a) Aluminium plate "$q = 1$," mode $M = 7$ numbered (1). (b) Plexiglas plate "$q = 2$," mode $I = 6$ numbered (1).

Eq. (22)]. The spatial structure of this mode SH7 (Figure 5) appears clearly in the aluminium plate (plate 1) along the x-axis, while the spatial structure of the incident mode SH6 (Figure 4) appears clearly in the same plate along the z-axis and the plexiglas plate along the x-axis (both modes present the same structure in the plexiglas plate along the z-axis). These observations are confirmed by the Fourier Transform diagrams on Figures 11(a) and 11(b), which show that the perturbation of the SH7 mode propagates forward [$(k_x, k_z) = (4.148, 6.320)$ numbered (1) in Figure 11(a)] and that the SH6 mode propagates backward [$(k_x, k_z) = (-5.868, 15.310)$ numbered (1) in

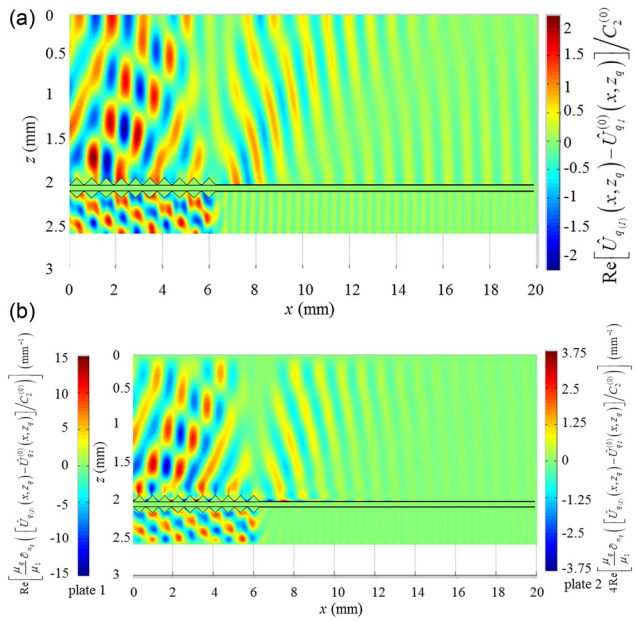

FIG. 12. Mapping of the real part of (a) the non-dimensional displacement field [Eq. (20)] and (b) the normalized stress field [Eq. (21)] of the incident SH-waves $I = 7$ for $fL_1 = 7.460\,\text{MHz mm}$ and $k_{x_M}^{(0)}L_1 = 8.297$ (dot $I = 7$ and $M = 6$ on Figure 9).

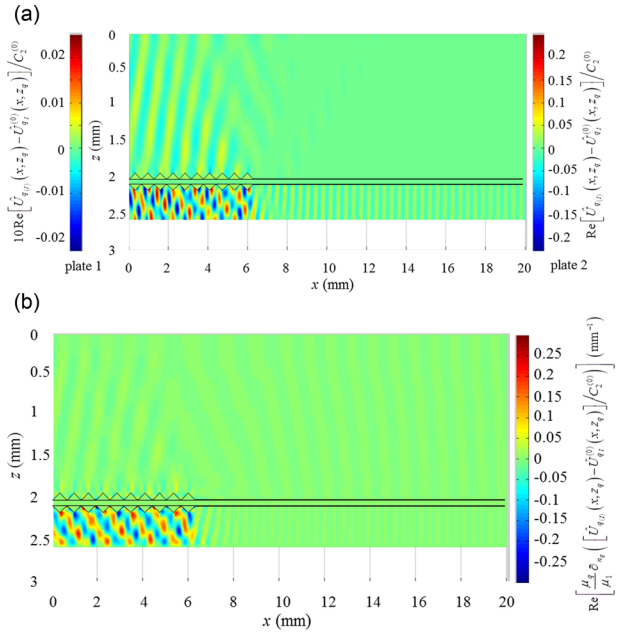

FIG. 13. Mapping of the real part of (a) the non-dimensional displacement field [Eq. (20)] and (b) the normalized stress field [Eq. (21)] of the incident SH-waves $I = 0$ for $fL_1 = 7.460$ MHz mm and $k_{x_M}^{(0)} L_1 = 32.471$.

Figure 11(b)], see Table II for the exact values of the couples (k_x, k_z). These results emphasized the role played by the phase-matching between these two modes $I = 6$ and $M = 7$, the amplitude of the perturbation of the other modes being clearly negligible. These results show that, despite the complexity of the coupling effects through the roughened layer of glue, the structures of the perturbations depend strongly on the nature of the incident SH-wave and on the phase-matching which involve both another SH-wave and the spatial period of the roughness. Note that the amplitude of the perturbed waves

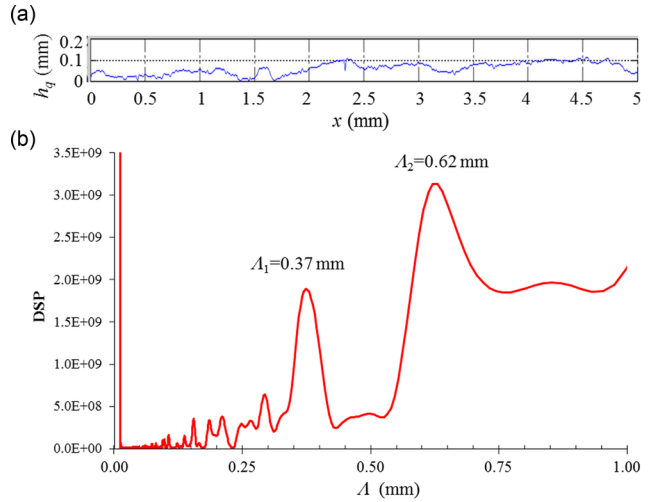

FIG. 15. Example of experimental pseudo-random profile (shot-blasting[12]) (a) and PSD of the profile (b).

is at least five times lower than those of the corresponding incoming wave and that, as expected, the field perturbation does not propagate significantly beyond the roughness $x > \ell$ [backward propagating wave perturbation, Eq. (22)]. Results presented below confirm the statements mentioned here (other results not presented herein show the same behaviors).

Figures 12(a) and 12(b) show, respectively, the mapping of the real parts of the displacement fields and stress fields perturbations of the incoming SH-wave $I = 7$, due to the scattering on the roughness, for $fL_1 = 7.460$ MHz mm and $k_{x_7}^{(0)} L_1 = 8.297$ (dot $I = 7$ and $M = 6$ on Figure 9). For a better visibility in Figure 12(b), the color contrast in the aluminium plate (plate 1) was enhanced by multiplying the amplitude by four (see the left scale for the aluminium plate and the right scale for the plexiglas plate). These results

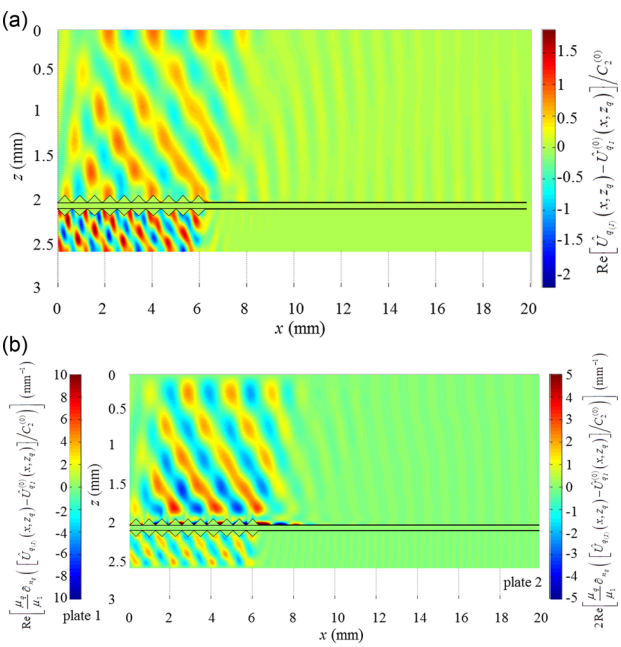

FIG. 14. Mapping of the real part of (a) the non-dimensional displacement field [Eq. (20)] and (b) the normalized stress field [Eq. (21)] of the incident SH-waves $I = 5$ for $fL_1 = 7.460$ MHz mm and $k_{x_5}^{(0)} L_1 = 13.672$ (no phase-matching).

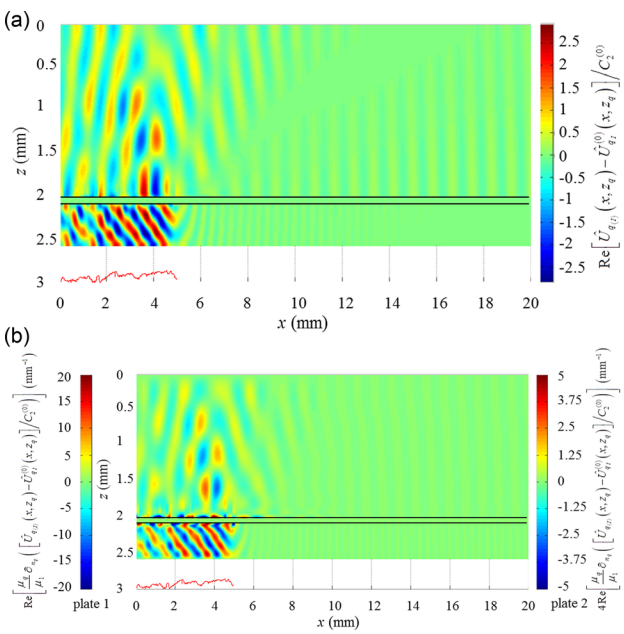

FIG. 16. Mapping of the real part of (a) the non-dimensional displacement field [Eq. (20)] and (b) the normalized stress field [Eq. (21)] of the incident SH-waves $I = 6$ for $fL_1 = 7.460$ MHz mm and $k_{x_M}^{(0)} L_1 = 11.737$ (dot $I = 6$ on Figure 9).

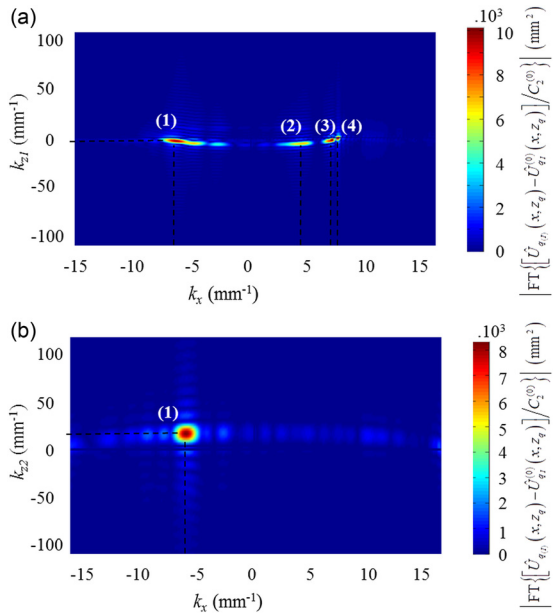

FIG. 17. Modulus of the two dimensional Fourier Transform of the map presented in Figure 16(a). (a) Aluminium plate "$q = 1$," modes $M = 5, 7, 4,$ and 3, respectively, numbered (1), (2), (3), and (4). (b) Plexiglas plate "$q = 2$," mode $I = 6$ numbered (1).

show that the behaviours are here analogue to those presented in Figure 10 (see Figures 4 and 5 for the results without roughness), More particularly, the perturbation present the spatial structure of both the incident SH-wave $I = 7$ and the coupled mode $M = 6$, which emphasize once more the role played by the phase-matching between these two modes SH7 and SH6 [see Eq. (22)]. The Fourier Transform diagrams (non presented here for brevity) confirm clearly these

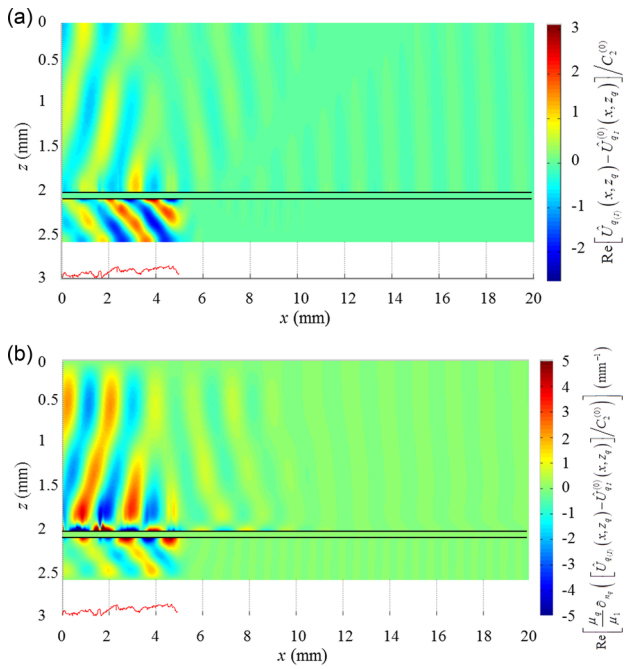

FIG. 18. Mapping of the real parts of (a) the non-dimensional displacement field [Eq. (20)] and (b) the normalized stress field [Eq. (21)] of the incident SH-wave $I = 4$ for $fL_1 = 4.560$ MHz mm and $k_{x_4}^{(0)} L_1 = 6.639$ (dot $I = 4$ and $M = 1$ on Figure 9).

results but it shows also the minor contribution of other modes (SH5, SH6, and SH7) in the neighbouring of the main modes. This can explain the complex structure which appears on the maps.

Figures 13(a) and 13(b) present the mapping of the real parts of the displacement fields perturbations (a) and the stress fields perturbations (b) of the incident SH-wave $I = 0$, created by the scattering on the corrugated surfaces, for $fL_1 = 7.460$ MHz mm and $k_{x_0}^{(0)} L_1 = 32.471$ (dot $M = 0$ on Figure 3). For a better visibility in Figure 13(a), the color contrast in the aluminum plate (plate 1) was enhanced by multiplying the amplitude by ten (see the left scale for the aluminium plate and the right scale for the plexiglas plate). As expected, the spatial periodicity along the x-axis of the incoming wave $I = 0$ (Figure 6) appears in the plexiglas plate (this mode is evanescent in the aluminium plate). A very small counter-propagating wave perturbation occurs in the aluminium plate (its amplitude increases towards the input), while a very small perturbation created along the roughness in the plexiglas plate propagates forwardly. This last perturbation results mainly from the contribution of SH6 mode (propagating backward) and the SH1 mode (propagation forward) which interfere with the SH0 mode propagating backward (these results are given by the Fourier Transform diagrams (non presented here)).

Figure 14 present the mapping of the real parts of the displacement fields perturbations (a) and the stress fields perturbations (b) of the incident SH-wave $I = 5$, created by the scattering on the corrugated surfaces, for $fL_1 = 7.460$ MHz mm and $k_{x_5}^{(0)} L_1 = 13.672$. For a better visibility in Figure 14(b), the color contrast in the plexiglas plate (plate 2) was enhance by multiplying the amplitude by two (see the left scale for the aluminium plate and the right scale for the plexiglas plate). As expected, the spatial periodicities of this incoming wave $I = 5$ appear clearly in the plexiglas plate, while the perturbation field involves an important effect of several modes or all the modes (at this frequency, the incident SH-wave $I = 5$ has not any phase-marching with any other SH-waves). These results are confirmed by the Fourier Transform diagram (not presented here).

2. Pseudo-random profile

In the next example, the roughness (in fact herein ridges) is assumed to have the pseudo-random profile shown in Figure 15(a), which represents a shot-blasting profile, with a depth $h(x) < 1.1$ mm and a length $\ell = 5$ mm. Its power spectral density (PSD) exhibits two spatial periods $\Lambda_1 \cong 0.372$ mm and $\Lambda_2 \cong 0.621$ mm (usually, in practice, rough surfaces exhibit a limited number of dominant spatial periodicities) (Figure 15(b)).

Figures 16(a) and 16(b) show, respectively, the mapping of the real part of the displacement and the stress fields perturbations, for the value $\Lambda_2 = 0.62$ mm of spatial pseudo-period mentioned above, which has the same value as the spatial period of the sawtooth profile mentioned previously, the working point being the one marked $I = 6$ (incident wave) in Figure 9. Then, the dispersion curves and the phonon ones considered here are those depicted in this figure,

and the phase-matching between the incident mode SH6 and the mode SH7 which occurs in the configuration presented in Figure 16 (pseudo-random profile) is the same as in the configuration presented in Figure 10 (periodic profile). For a better visibility in Figure 16(b), the color contrast in the plexiglas plate (plate 2) was enhanced by multiplying the amplitude by four (see the left scale for the aluminium plate and the right scale for the plexiglas plate). As expected, the structure of the perturbation field in Figures 16(a) and 16(b) shows the same spatial periodicities (SH6 and SH7), in both directions x and z, as the structure of the perturbation field in Figures 10(a) and 10(b). This is confirmed by the Fourier Transform diagrams (Figures 17(a) and 17(b)), with SH6 numbered (1) in Figure 17(b) and SH7 numbered (2) in Figure 17(a). But the global structure appears slightly different because several SH modes are involved: mainly SH5 (numbered (1) in Figure 17(a), SH4 (numbered 3), and SH3 (numbered 4) propagating forwardly. As a result, the structure of the diffracted field would permit to control the values of the pseudo-period.

Figures 18(a) and 18(b) present the mapping of the real parts of the displacement fields perturbations (a) and the stress fields perturbations (b) of the incident SH-wave $I = 4$, created by the scattering on the pseudo-random profile for $fL_1 = 4.560\,\text{MHz mm}$ and $k_{x_4}^{(0)}L_1 = 6.639$ (dot $I = 4$ and $M = 1$ on Figure 9). A phase-matching occurs between this incident mode SH4 and the mode SH1. As expected, the spatial structure of the incident mode SH4 appears in both plates, the mode SH1 being superposed to the mode SH4 in the plexiglas plate only, because it is evanescent in the aluminium plate. These results are confirmed by the Fourier Transform diagram (not presented here). Once more, this result emphasized the importance of the phase-matching when it occurs with a periodic or a pseudo-periodic roughness.

VI. SUMMARY, CONCLUSION, AND PROSPECT

An analytical model for describing the scattering effects of roughness on the behavior of SH-waves propagating inside two plates stick together with a layer of glue has been worked out, which account for the shape and the depth of the roughness (among other parameters). While this analytical modelling could appears somewhat cumbersome, the numerical calculations are in fact simple and rapid to handle. The results demonstrate that the extracted parameters show the expected sensitivity to the characteristics of the roughness profiles. Thus, the predictions of this model should be useful to describe phenomena in a variety of plates and roughness profiles.

So far, in our knowledge, no previous analytical results could be used as a preliminary test of the effectiveness of the model. As well, no experimental and numerical attempt was carried out to validate its prediction capability. Therefore, such experimental and numerical work is likely to be the subject of investigation in a near future.

ACKNOWLEDGMENTS

Support from CNRS through the research group GDRE-2501 "Wave Propagation in Complex Media for Quantitative and Non Destructive Evaluation" is gratefully acknowledged. The authors also want to thank their colleagues in the "Fédération d'Acoustique du Nord Ouest" (FANO, FR CNRS 3110) for their helpful discussions. This work was supported by the ANR grant ISABEAU (project ANR 12-BS-09-0022-01). The authors are indebted to the reviewers who help them to improve substantially the manuscript.

APPENDIX A: TWO PLATES WITH SMOOTH SURFACES AND WITH A LAYER OF GLUE (ZERO ORDER APPROXIMATION): CONTINUITY CONDITIONS AT THE INTERFACES BETWEEN THE PLATES AND THE LAYER OF GLUE

The behaviour of the glue is expressed by the classical spring-like model with a spring stiffness (μ_g/L_g) (7b), which takes the following form when the interfaces are not roughened (q = 1, 2):

$$\mu_q \partial_{z_q} \hat{U}_q^{(0)} = -\mu_{s\neq q} \partial_{z_{s\neq q}} \hat{U}_{s\neq q}^{(0)} = \frac{\mu_g}{L_g}\left[\hat{U}_{s\neq q}^{(0)}(x', L_s/2) - \hat{U}_q^{(0)}(x', L_q/2)\right]. \quad \text{(A1)}$$

Accounting for the expression of the displacement field (8a), these equations lead to the continuity conditions which can be written as

$$\begin{bmatrix} a_{11} & a_{12} \\ a_{21} & a_{22} \end{bmatrix} \begin{pmatrix} C_1^{(0)} \\ C_2^{(0)} \end{pmatrix} = \begin{pmatrix} 0 \\ 0 \end{pmatrix}, \quad \text{(A2)}$$

where

$$a_{11} = e^{ik_{z_1}^{(0)}L_1/2}\left[\cos\left(k_{z_1}^{(0)}L_1\right) + \frac{\mu_1 k_{z_1}^{(0)}}{\mu_g(2/L_g)}\sin\left(k_{z_1}^{(0)}L_1\right)\right], \quad \text{(A3a)}$$

$$a_{12} = -e^{ik_{z_2}^{(0)}L_2/2}\left[\cos\left(k_{z_2}^{(0)}L_2\right) + \frac{\mu_2 k_{z_2}^{(0)}}{\mu_g(2/L_g)}\sin\left(k_{z_2}^{(0)}L_2\right)\right], \quad \text{(A3b)}$$

$$a_{21} = \mu_1 k_{z_1}^{(0)} e^{ik_{z_1}^{(0)}L_1/2}\sin\left(k_{z_1}^{(0)}L_1\right), \quad \text{(A3c)}$$

$$a_{22} = \mu_2 k_{z_2}^{(0)} e^{ik_{z_2}^{(0)}L_2/2}\sin\left(k_{z_2}^{(0)}L_2\right). \quad \text{(A3d)}$$

The determinant of Equation (A2) must vanish, which gives the dispersion equation (9).

APPENDIX B: GRAM-SCHMIDT METHOD FOR ORTHONORMALISING THE SET OF SH MODES

The method for orthonormalising the set of SH-modes takes the following form:

$$\psi_{q_m}(z_q) = \psi_{q_m}^{\perp}(z_q)/\langle\psi_{q_m}^{\perp}|\psi_{q_m}^{\perp}\rangle^{1/2}, \quad \text{(B1)}$$

where

$$\psi_{q_m}^{\perp}(z_q) = \varphi_{q_m}(z_q) - \sum_{j=0}^{m-1}\langle\varphi_{q_m}|\psi_{q_j}\rangle\psi_{q_j}(z_q), \quad \text{(B2)}$$

and

$$\varphi_{q_m}(z_q) = U^{(0)}_{q_M}(x_q, z_q)/\left[2C^{(0)}_q \exp\left(\mathrm{i}k^{(0)}_{z_q M} L_q/2\right) \exp\left(-\mathrm{i}k^{(0)}_{x_M} x\right)\right] = \cos\left[k^{(0)}_{z_q M}(z_q + L_q/2)\right], \tag{B3}$$

with

$$\psi_{q_0}(z_q) = \varphi_{q_I}(z_q)/\langle \varphi_{q_I} | \varphi_{q_I} \rangle^{1/2}, \tag{B4}$$

the bracket $\langle f|g\rangle = \int_{-L_q/2}^{L_q/2} f(z_q)\, g^*(z_q)\, \mathrm{d}z_q$ denoting the inner product in the intervals $z_q \in (-L_q/2, L_q/2)$.

Note that, instead of computing this process, we used the equivalent "modified Gram-Schmidt" process, in order to avoid unacceptable loss of orthogonality due to rounding errors.[38]

APPENDIX C: INTEGRAL FORMULATION, EXPANSION ON ORTHONORMAL FUNCTIONS, AND BORN APPROXIMATION

Note that the integral in the right hand side of Equation (15a) vanishes outside the roughened domain $(x > \ell)$ and accounting for the behaviour of the glue [Equation (7b)], namely, here

$$\partial_{n'_q} \hat{U}_{q M}(x', Z'_q) \cong [\mu_g/(\mu_q \ell_g)][\hat{U}_{s \neq q_M}(x', Z'_s) - \hat{U}_{q_M}(x', Z'_q)],$$

Equation (15a) can be written as follows:

$$\left.\begin{array}{ll} (x, z_q) \in (D_q), & \hat{U}_{q_{(I)}}(x, z_q) \\ (x, z_q) \in (D_{q_0} - D_q), & 0 \end{array}\right\} \cong \hat{U}^{(0)}_{q_I}(x, z_q) + \{\hat{H}_{q_I}(x, z_q) + \hat{E}_{q_I}(x, z_q)\}, \tag{C1}$$

where

$$\hat{H}_{q_I}(x, z_q) = -\int_0^{\ell} \{\delta_2[\hat{U}_{q_I}(x', Z'_q)\partial_{n'_q} G_q(x, z_q; x', Z'_q)]\}\, \mathrm{d}x', \tag{C2}$$

$$\hat{E}_{q_I}(x, z_q) = -\frac{\mu_g}{\mu_q}\int_0^{\ell} \{\delta_3[\ell_g^{-1}(x')(\hat{U}_{q_I}(x', Z'_q) - \hat{U}_{s \neq q_I}(x', Z'_s))G_q(x, z_q; x', Z'_q)]\}\mathrm{d}x', \tag{C3}$$

with

$$\delta_2[\hat{U}_{q_I}(x', Z'_q)\partial_{n'_q} G_q(x, z_q; x', Z'_q)] = \hat{U}_{q_I}(x', Z'_q)\partial_{n'_q} G_q(x, z_q; x', Z'_q) - \hat{U}^{(0)}_{q_I}(x', L_q/2)\partial_{z'_q} G_q(x, z_q; x', L_q/2), \tag{C4a}$$

and

$$\delta_3[\ell_g^{-1}(x')(\hat{U}_{q_I}(x', Z'_q) - \hat{U}_{s \neq q_I}(x', Z'_s))G_q(x, z_q; x', Z'_q)] = \ell_g^{-1}(x')(\hat{U}_{q_I}(x', Z'_q) - \hat{U}_{s \neq q_I}(x', Z'_s))G_q(x, z_q; x', Z'_q) - L_g^{-1}(x')(\hat{U}^{(0)}_{q_I}(x', L_q/2) - \hat{U}^{(0)}_{s \neq q_I}(x', L_s/2)) \times G_q(x, z_q; x', L_q/2). \tag{C4b}$$

Expression (C2) represents the scattering effects due, respectively, to the shape profile and the depth of the roughness at the interface between the plate q considered and the layer of glue, and expression (C3) represents the perturbation on the coupling between the plates through the layer of glue (both due also to the shape profile and the depth of the roughness) which account for the effect of the thickness of the layer of glue (depending on the x-coordinate), the limits of integration $x' = 0$ and $x' = \ell$ in these expressions being those of the interval where the roughness does not vanish. Note that one can anticipate accurate results in as much as the integrands can be considered as small perturbations (the depth of the ridges is assumed to be small on both the wavelength scale and the thickness of the plates scale).

In multiplying Equation (C1) by the orthonormal functions $\psi_{q_{m_{(I)}}}(z_q)$ [see Appendix B] and integrating over the intervals $z_q \in (-L_q/2, Z_q)$, the left hand side and the first term in the right hand side of the equation become

$$\int_{-L_q/2}^{Z_q} [\hat{U}_{q_{(I)}}(x, z_q) - \hat{U}^{(0)}_{q_I}(x, z_q)]\, \psi_{q_{m_{(I)}}}(z_q)\, \mathrm{d}z_q = \left\{\int_{-L_q/2}^{L_q/2} - \int_{Z_q}^{L_q/2}\right\} \sum_{\nu} [\hat{A}_{q_{\nu_{(I)}}}(x) - \hat{A}^{(0)}_{q_{\nu_{(I)}}}(x)] \times \psi_{q_{\nu_{(I)}}}(z_q)\psi_{q_{m_{(I)}}}(z_q)\mathrm{d}z_q, \tag{C5}$$

after relying on Equation (16) [i.e., the expansion of the displacement field $\hat{U}_{q_{(I)}}$ and also $\hat{U}^{(0)}_{q_{(I)}}$ (with the coefficients $\hat{A}^{(0)}_{q_{\nu_{(I)}}}$) on the orthonormal functions $\psi_{q_{\nu_{(I)}}}(z_q)$]. Then, Equation (C1) can be written as follows:

$$\left\{\int_{-L_q/2}^{L_q/2} - \int_{Z_q}^{L_q/2}\right\} \sum_{\nu} [\hat{A}_{q_{\nu_{(I)}}}(x) - \hat{A}^{(0)}_{q_{\nu_{(I)}}}(x)] \times \psi_{q_{\nu_{(I)}}}(z_q)\psi_{q_{m_{(I)}}}(z_q)\mathrm{d}z_q = \int_{-L_q/2}^{Z_q} [\hat{H}_{q_I}(x, z_q) + \hat{E}_{q_I}(x, z_q)]\, \psi_{q_{m_{(I)}}}(z_q)\mathrm{d}z_q, \tag{C6}$$

the endpoints Z'_q depending on the coordinate x'.

Therefore, we assume Born approximation in the terms of order of magnitude of the thickness $h_q = L_q/2 - Z_q$ of the roughness and its slope (the higher order terms being neglected); in other words, we neglect the integral over the very small interval $[Z_q, L_q/2]$ of length ℓ_g of the small factor $[\hat{A}_{q_{\nu_{(I)}}}(x) - \hat{A}^{(0)}_{q_{\nu_{(I)}}}(x)]$ in the left hand side of Eq. (C6), and, in the small terms in the right hand side of this equation, we substitute $\hat{U}^{(0)}_{q_I}$ for $\hat{U}_{q_{(I)}}$ and we approximate

$$\langle f_1 \| f_2 \rangle = \int_{-L_q/2}^{Z_q} f_1(z_q) f_2(z_q)\, \mathrm{d}z_q = \left\{\int_{-L_q/2}^{L_q/2} - \int_{Z_q}^{L_q/2}\right\} f_1(z_q) f_2(z_q)\, \mathrm{d}z_q, \tag{C7a}$$

by

$$\langle f_1 \| f_2 \rangle \cong \int_{-L_q/2}^{L_q/2} f_1(z_q) f_2(z_q) \mathrm{d}\, z_q. \tag{C7b}$$

The last approximation means that the loss of orthogonality of the Gram-Schmidt orthogonal functions over the interval $[-L_q/2, L_q/2]$ in the left hand side of Eq. (C6). Namely,

$$\int_{Z_q}^{L_q/2} \psi_{q_{\nu_{(I)}}}(z_q) \psi_{q_{m_{(I)}}}(z_q) \mathrm{d}\, z_q, \tag{C8}$$

is negligible.

Then taking into account the orthogonality properties of the functions $\psi_{q_{m_{(I)}}}(z_q)$ over the interval $[-L_q/2, L_q/2]$ yield the following relationship between the incident field [coefficients $\hat{A}^{(0)}_{q_{m_I}}(x)$] and the unknown coefficients $\hat{A}_{q_{m_{(I)}}}(x)$:

$$\hat{A}_{q_{m_{(I)}}}(x) - \hat{A}^{(0)}_{q_{m_I}}(x) \cong \hat{\tilde{H}}_{q_{m_{(I)}}}(x) + \hat{\tilde{E}}_{q_{m_{(I)}}}(x), \tag{C9a}$$

where

$$\begin{aligned} \hat{A}^{(0)}_{q_{mI}}(x) &\cong \langle \hat{U}^{(0)}_{q_I}(x, z_q) \| \psi_{q_m}(z_q) \rangle \\ &= \langle \hat{U}^{(0)}_{q_I}(x, z_q) \| \psi_{q_{m=0}}(z_q) \rangle, \end{aligned} \tag{C9b}$$

$$\begin{aligned} \hat{\tilde{H}}_{q_{m_{(I)}}}(x) \cong -\int_0^{\ell} \{ \delta_2 [\hat{U}^{(0)}_{q_I}(x', Z'_q) \\ \times \langle \partial_{n'_q} G_q(x, z_q; x', Z'_q) \| \psi_{q_m}(z_q) \rangle] \}\, \mathrm{d}x', \end{aligned} \tag{C9c}$$

$$\begin{aligned} \hat{\tilde{E}}_{q_{m_{(I)}}}(x) \cong -\frac{\mu_g}{\mu_q} \int_0^{\ell} \left\{ \delta_3 \left[\ell_g^{-1} \left(\hat{U}^{(0)}_{q_I}\left(x', Z'_q\right) - \hat{U}^{(0)}_{s \neq q_I}(x', Z'_s) \right) \right. \right. \\ \left. \left. \times \left\langle G_q\left(x, z_q; x', Z'_q\right) \| \psi_{q_m}(z_q) \right\rangle \right] \right\} \mathrm{d}x'. \end{aligned} \tag{C9d}$$

Finally, in each plate labelled "q," the displacement field perturbation due to the scattering of the incident SH-wave (labelled "I") on the roughened surfaces is given by Equation (17a).

It is worthwhile commenting that the Green function in the integrals in expressions (17b) and (17c) has integrand singularities, but the limits of integrations are finite. In expression (17c), the integrand tends logarithmically to infinity as the argument u of the Green function tends to zero, but the integral converges. In expression (17b), the Green function is differentiated with respect to x and z (first order derivatives) and then the integrand behaves as $(1/u)$ as $u \to 0$. Therefore, in order to ensure efficiency of the numerical calculations, which are handled in using MATLAB® software, the derivatives of the Green function in the integrands are removed on using first the reciprocity property $\partial_{x'_q} G_q = -\partial_{x_q} G_q$ and second the first order Taylor expansions around the points Z_q and $L_q/2$ [avoiding integration by part then the derivatives of the orthogonal functions $\psi_{q_{m_{(I)}}}(z_q)$]. Therefore, the expressions for $\hat{\tilde{H}}_{q_{m_{(I)}}}(x)$ and $\hat{\tilde{E}}_{q_{m_{(I)}}}(x)$ used in the computational process, which involves only the Green function not its derivatives, take the following form:

$$\begin{aligned} \hat{\tilde{H}}_{q_{m_{(I)}}}(x) = \partial_x \int_0^{\ell} \hat{U}^{(0)}_{q_I}\left(x', Z'_q\right) N_q^{-1}(x') \left(\mathrm{d}_{x'}\, h_q(x') \right) \\ \times \langle G_q\left(x, z_q; x', Z'_q\right) \| \psi_{q_m}(z_q) \rangle \mathrm{d}x' \\ + \int_0^{\ell} \left[\hat{U}^{(0)}_{q_I}(x', L_q/2) - \frac{\hat{U}^{(0)}_{q_I}(x', Z'_q)}{N_q(x')} \right] \\ \times \frac{1}{h_q(x')} \langle [G_q(x, z_q; x', z'_q = L_q/2) \\ - G_q(x, z_q; x', z'_q = Z'_q)] \| \psi_{q_m}(z_q) \rangle\, \mathrm{d}x', \end{aligned} \tag{C10a}$$

$$\begin{aligned} \hat{\tilde{E}}_{q_{m_{(I)}}}(x) = -\int_0^{\ell} \{ \delta_2 [\partial_{n'_q} \hat{U}^{(0)}_{qI}(x', z'_q = Z'_q) \\ \times \langle G_q(x, z_q; x', z'_q = Z'_q) \| \psi_{q_m}(z_q) \rangle] \} \mathrm{d}x', \end{aligned} \tag{C10b}$$

after relying on Equation (17e).

[1] H. Matt, I. Bartoli, and F. Lanza di Scalea, "Ultrasonic guided wave monitoring of composite wing skin-to-spar bonded joints in aerospace structures," J. Acoust. Soc. Am. **118**(4), 2240–2252 (2005).

[2] A. C. Okafor, N. Singh, U. E. Enemuoh, and S. V. Rao, "Design, analysis and the performance of adhesively bonded composite patch repair of cracked aluminium aircraft panels," Compos. Struct. **71**, 258–270 (2005).

[3] T. A. Barnes and I. R. Pashby, "Joining techniques for aluminium space-frame used in automobiles. Part II-adhesive bonding and mechanical fasteners," J. Mater. Process. Technol. **99**(1), 72–79 (2000).

[4] Z. Su, L. Ye, and Y. Lu, "Guided Lamb waves for identification of damage in composite structures: A review," J. Sound Vib. **295**, 753–780 (2006).

[5] M. Castaings and B. Hosten, "Guided waves propagating in sandwich structures made of anisotropic, viscoelastic, composite materials," J. Acoust. Soc. Am. **113**(5), 2622–2634 (2003).

[6] M. Castaings, "SH ultrasonic guided waves for the evaluation of interfacial adhesion," Ultrasonics **54**, 1760–1775 (2014).

[7] D. Qing-tian and Y. Zhi-chun, "Propagation of guided waves in bonded composite structures with tapered adhesive layer," Appl. Math. Modell. **35**, 5369–5381 (2011).

[8] N. Quaegebeur, P. Micheau, P. Masson, and M. Castaings, "Methodology for optimal configuration in structural health monitoring of composite bonded joints," Smart Mater. Struct. **21**, 105001–105011 (2012).

[9] R. Leiderman, A. M. B. Braga, and P. E. Barbone, "Scattering of ultrasonic waves by defective adhesion interfaces in submerged laminated plates," J. Acoust. Soc. Am. **118**, 2154–2181 (2005).

[10] R. Leiderman, P. E. Barbone, and A. M. B. Braga, "Reconstructing the adhesion stiffness distribution in a laminated elastic plate: Exact and approximate inverse scattering solutions," J. Acoust. Soc. Am. **122**(4), 1906–1916 (2007).

[11] L. Singher, Y. Segal, and J. Shamir, "Interaction of a guided wave with a nonuniform adhesion bond," Ultrasonics **35**, 385–391 (1997).

[12] R. Leiderman and D. Castello, "Scattering of ultrasonic waves by heterogeneous interfaces: Formulating the direct scattering problem as a least-squares problem," J. Acoust. Soc. Am. **135**(1), 5–16 (2014).

[13] H. Lourmes, "Etude des assemblages collés par ondes guidées ultrasonores: étude expérimentale et modélisation par éléments finis," Ph.D. thesis (Université Bordeaux 1, 2009).

[14] V. Vlasie, S. de Barros, M. Rousseau, L. Champaney, H. Duflo, and B. Morvan, "Mechanical and acoustical study of a structural bond: Comparison theory/numerical simulations/experiment," Eur. J. Mech. A/Solids **25**, 464–482 (2006).

[15]S. Banerjee and T. Kundu, "Elastic wave propagation in sinusoidally corrugated waveguides," J. Acoust. Soc. Am. **119**(4), 2006–2017 (2006).
[16]M. A. Hawwa, "Acoustic/elastic stop-band interaction in waveguides involving two periodicities," J. Acoust. Soc. Am. **102**(1), 137–142 (1997).
[17]M. A. Hawwa and O. Asfar, "Coupled mode analysis of love waves in a filter film with periodically corrugated surfaces," IEEE Trans. Ultrason., Ferroelectr., Freq. Control **41**(1), 13–18 (1994).
[18]T. Krasnova, P.-A. Jansson, and A. Boström, "Ultasonic wave propagation in an anisotropic cladding with a wavy interface," Wave Motion **41**, 163–177 (2005).
[19]S. S. Singh, "Love wave at a layer medium bounded by irregular boundary surfaces," J. Vib. Control **17**(5), 789–795 (2011).
[20]N. F. Declercq, "Inhomogeneous waves obliquely incident on a periodic structure," Acta Acust. **100**, 1–4 (2014).
[21]Z. Tao, W. He, Y. Xiao, and X. Wang, "Wide forbidden band induced by the interference of different transverse acoustic standing-wave modes," Appl. Phys. Lett. **92**, 121920 (2008).
[22]A. R. McGurn and A. A. Maradudin, "Speckle correlations in the light scattered by a dielectric film with a rough surface: Guided wave effects," Phys. Rev. B **58**(8), 5022–5031 (1998).
[23]W. A. Kuperman and H. Schmidt, "Rough surface elastic wave scattering in a horizontally stratified ocean," J. Acoust. Soc. Am. **79**(6), 1767–1777 (1986).
[24]V. E. Ostashev, D. K. Wilson, and S. N. Vecherin, "Waveguide sound propagation in a turbulent atmosphere above randomly rough ground," Proc. Meet. Acoust. **14**, 045004 (2012).
[25]D. Cerniglia, N. Montinaro, and V. Nigrelli, "Detection of disbonds in multi-layered structures by laser ultrasonic technique," J. Adhes. **84**, 811–829 (2008).
[26]J. C. Samuels, "On propagation of waves in slightly rough ducts," J. Acoust. Soc. Am. **31**(3), 319–325 (1959).
[27]M. Spivack, "Sound propagation in an irregular two-dimensional waveguide," J. Acoust. Soc. Am. **101**(3), 1250–1255 (1997).
[28]J. A. Sanchez-Gil, V. Freilikher, A. A. Maradudin, and I. V. Yurkevich, "Reflection and transmission of waves in surface-disordered waveguides," Phys. Rev. B **59**(8), 5915–5925 (1999).
[29]T. Valier-Brasier, C. Potel, M. Bruneau, D. Leduc, B. Morvan, and J.-L. Izbicki, "Coupling of shear acoustic waves by gratings: Analytical and experimental analysis of spatial periodicity effects," Acta Acust. **97**(5), 717–727 (2011).
[30]J. Koreck, C. Valle, J. Qu, and L. J. Jacob, "Computational characterization of adhesive layer properties using guided waves in bonded plates," J. Nondestruct. Eval. **26**, 97–105 (2007).
[31]R. Seifried, L. J. Jacobs, and J. Qu, "Propagation of guided waves in adhesive bonded components," NDT & E Int. **35**, 317–328 (2002).
[32]M. V. Predoi, M. Castaings, B. Hosten, and C. Bacon, "Wave propagation along transversely periodic structures," J. Acoust. Soc. Am. **121**, 1935–1952 (2007).
[33]Z. Hong, "Analysis of guided waves in adhesively bonded composite structures," J. Appl. Sci. **13**(22), 5298–5308 (2013).
[34]T. Valier-Brasier, C. Potel, and M. Bruneau, "Modes coupling of shear acoustic waves polarized along a one-dimensional corrugation on the surfaces of an isotropic solid plate," Appl. Phys. Lett. **93**, 164101 (2008).
[35]T. Valier-Brasier, C. Potel, and M. Bruneau, "Shear acoustic waves polarized along the ridged surface of an isotropic solid plate: Mode coupling effects due to the shape profile," J. Appl. Phys. **108**(7), 074910 (2010).
[36]J. P. Jones and J. S. Whitter, "Wave in a flexible bounded interface," J. Appl. Mech. **34**, 905–909 (1967).
[37]M. Schoenberg, "Elastic wave behavior across elastic linear slip interfaces," J. Acoust. Soc. Am. **68**(5), 1516–1521 (1980).
[38]L. Giraud, J. Langou, and M. Rozloznik, "On the loss of orthogonality in the Gram-Schmidt orthogonalization process," CERFACS, Technical Report No. TR/PA/03/15; Comput. Math. Appl. **50**, 1069–1075 (2005).
[39]P. M. Morse and H. Feshbach, *Methods of Theoretical Physics, Part II* (McGraw-Hill, New-York, 1953).
[40]M. Bruneau and T. Scelo (translator and contributor), *Fundamentals of Acoustics* (ISTE, UK and USA, 2006).